Surface ferromagnetism in the chiral topological semimetal CoSi

N. N. Orlova, A. A. Avakyants ⓘ, A. V. Timonina, N. N. Kolesnikov ⓘ, and E. V. Deviatov
Institute of Solid State Physics of the Russian Academy of Sciences, Chernogolovka, Moscow District,
2 Academician Ossipyan str., 142432 Russia

Despite the chiral topological semimetal CoSi being known as bulk diamagnetic, it shows unusual surface ferromagnetism of debatable origin. The ferromagnetic ordering has been attributed to the distorted bonds, the superlattice of ordered vacancies, or even to topological surface textures due to the spin polarization in the neighboring Fermi arcs. We experimentally compare magnetization reversal curves for initially oxidized CoSi single crystals and cleaved samples with a fresh, oxide-free surface. While the oxidized CoSi samples do not show sizable ferromagnetism, the fresh CoSi surface gives a strong ferromagnetic response, which is accompanied by the pronounced modulation of the angle dependence of magnetization, as it can be expected for easy and hard axes in a ferromagnet. In addition to the first order reversal curves analysis, this observation allows us to distinguish between different mechanisms of the ferromagnetic ordering in CoSi single crystals. We conclude that the surface states-induced Ruderman-Kittel-Kasuya-Yosida (RKKY) interaction between distorted bonds near the sample surface is responsible for the strong ferromagnetic multidomain behavior for freshly cleaved samples.

I. INTRODUCTION

The concept of a chiral topological semimetal [1–3] is usually regarded as modification of a Weyl one by additionally broken mirror symmetry. While Weyl semimetals are characterized by multiple pairs of Weyl nodes with small separation in momentum space [4], there is only one pair of chiral nodes of opposite Chern numbers with large separation in chiral semimetals, which results in extremely long surface Fermi arcs [5,6]. Chiral topological semimetals also host new types of massless fermions with a large topological charge [7,8], which lead to numerous exotic physical phenomena like unusual magnetotransport [9], lattice dynamics [10], and a quantized response to circularly polarized light [11].

Chiral crystals are known, e.g., as monosilicides of Cr, Mn, Fe, and Co with the simple cubic B20 crystal structure [12–15]. Chiral symmetry is provided by the neutral 2_1 screw axis in the $P2_13$ space group [16]. Among these materials, CoSi is the most investigated one, so the bulk band structure and the presence of long surface Fermi arcs have been experimentally confirmed for CoSi [5,17–19].

One can expect a complicated response of topological semimetals on the external magnetic field due to the spin-momentum locking and, therefore, spin polarization of topological surface states. For example, spin polarization of the Fermi arcs in TaAs lies completely in the plane of the (001) surface and reaches 80% [20]. For the chiral topological semimetal CoSi, recent theoretical studies have shown that the spin-orbit interaction lifts the spin degeneracy of the surface states leading to their in-plane spin polarization on the (001) surface, with strongly correlated and predominantly antiparallel spin textures in the neighboring Fermi arcs [21]. In general, spin textures are known in magnetic materials as surface skyrmions [12,22–29] or spin helix structures [30,31].

Among the family of chiral crystals, MnSi is a ferromagnet with known low-temperature helimagnetic order and skyrmion magnetism near the Curie temperature [13], FeSi is a small-gap semiconductor with an anomalous temperature-dependent magnetic moment [32], while CoSi is a diamagnetic semimetal [33,34]. In the latter case, unusual surface ferromagnetism is reported for nanowires, policrystalline films [16,35,36], or even CoSi single crystals [37]. Skyrmion lattice has been experimentally shown for the polycrystalline CoSi films [16,38,39]. Also, unconventional magnon modes have been reported as a joint effect of surface ferromagnetism and spin-orbit coupling in CoSi [40].

For the CoSi surface ferromagnetism, there is no clear understanding of the ordering mechanism. The Curie point is near room temperature ($T_c = 328$ K), which is the highest one among all B20-type ferromagnets [16]. One of the mechanisms is due to the distorted bonds: the transition metal (Co) d-orbital electron spin-up and spin-down populations become asymmetric from the exchange interactions near the CoSi surface [35,36]. As an alternative, the superlattice of ordered vacancies is considered as a source of ferromagnetic ordering [36]. Topological surface textures should also be considered due to the spin polarization in the neighboring Fermi arcs [21,41]. Moreover, the surface states-induced Ruderman-Kittel-Kasuya-Yosida (RKKY) interaction is expected to be available [42–44] when the topological surface states couple with the lattice-related ordering (e.g., the above-mentioned distorted bonds or ordered vacancies). Thus, one should to have a keystone experiment to distinguish between the different proposed mechanisms.

Here, we experimentally compare magnetization reversal curves for initially oxidized CoSi single crystals and cleaved samples with a fresh, oxide-free surface. While the oxidized CoSi samples do not show sizable ferromagnetism, the fresh
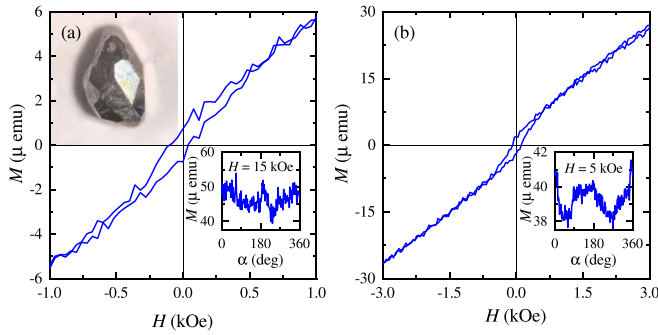
FIG. 1. Magnetization curves $M(H)$ at 100 K temperature for two initially oxidized CoSi crystals, 3.91 mg and 2.52 mg for (a) and (b), respectively. The qualitative behavior is very similar, it well-corresponds to the known one [16,34–37]. The main $M(H)$ dependence corresponds to the paramagnetic response, $M(H)$ does not demonstrate any clear orientation dependence, as depicted in the insets. The signal amplitude at fixed magnetic field does not scale with the sample mass, so $M(H)$ mostly reflects the contribution of the surface Co oxides [52,53], despite a weak hysteresis within ± 1 kOe interval.
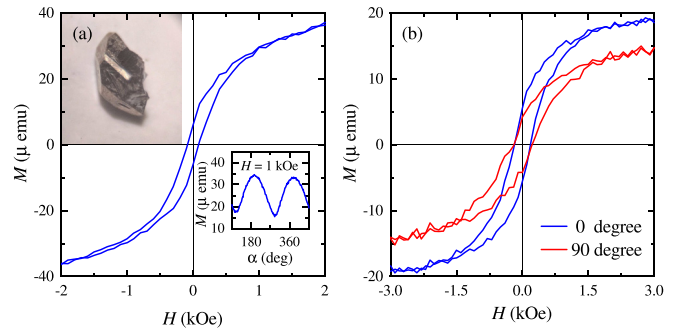

FIG. 2. Ferromagnetic response from the fresh CoSi surface. The initial samples from Fig. 1 are cleaved on smaller fragments, 1.86 mg and 0.48 mg in (a) and (b), respectively. Both samples demonstrate one order of magnitude increase in M value; there is now prominent hysteresis within ± 2 kOe field range, which is accompanied by well-defined $M(H)$ saturation in higher fields. Inset to (a) shows angle dependence of magnetization $M(\alpha)$ with 180° periodic modulation, reflecting well-defined easy and hard axes in a ferromagnet. For the second sample in (b), the angle dependence is shown as two hysteresis loops for these two (easy and hard) field orientations.

CoSi surface gives a strong ferromagnetic response, which is accompanied by the pronounced modulation of the angle dependence of magnetization, as it can be expected for easy and hard axes in a ferromagnet. This observation is compared with the expected one for different mechanisms of the ferromagnetic ordering in CoSi.

II. SAMPLES AND TECHNIQUES

CoSi single crystals are obtained in a two-step process. The initial CoSi material was synthesized from cobalt and silicon powders by 10°C/h heating in evacuated silica ampules up to 950°C. The ampules were held at this temperature for two weeks and then cooled down to room temperature at 6°C/h rate. The obtained material was identified as CoSi with some traces of SiO$_2$ by x-ray analysis. Afterward, CoSi single crystals are grown from this initial load by iodine transport in evacuated silica ampules at 1000°C. X-ray diffractometry demonstrates cubic structure of the crystals, also x-ray spectral analysis confirms equiatomic ratio of Co and Si in the composition, without any SiO$_2$ traces. The quality of our CoSi crystals have been verified in a number of transport experiments [40,45,46].

To investigate magnetic properties of small CoSi single crystal samples, we use Lake Shore Cryotronics 8604 VSM magnetometer, equipped with nitrogen flow cryostat. A CoSi crystal is mounted to the sample holder by a low temperature grease, which has been tested to have a negligible magnetic response.

For the magnetization measurements, we use small (about 2.52–3.91 mg) CoSi single crystals, see the inset to Fig. 1(a) as an example. Initially, the crystals have been exposed to air (at ambient conditions) for several months, so the surface is covered by the native oxide. After the first step of magnetization measurements, every crystal has been cleaved to obtain a fresh, oxide-free surface, see the inset to Fig. 2(a). The cleaved

sample has been immediately mounted to the flow cryostate for the second step of magnetization measurements.

We obtain hysteresis loops at different temperatures by the standard method of the magnetic field, gradually sweeping between two opposite saturation values. We also perform first order reversal curves (FORC) analysis, which provides additional information on the magnetic phases and their interaction. For the FORC analysis the magnetization curves are recorded as a two-dimensional map with the reversal field H_r and demagnetization field H [47,48]. Then the obtained $\rho(H, H_r)$ map is usually redrawn in (H_u, H_c) coordinates, where $H_u = \frac{1}{2}(H + H_r)$ is the interaction field and $H_c = \frac{1}{2}(H - H_r)$ is the coercivity field, see Refs. [47,49] for details.

The FORC density distribution $\rho(H_u, H_c)$ is known to be convenient for analysis [50,51]. The closed contours of the density distribution peak are usually associated with single-domain regime, while multidomain material gives open contours that diverge towards the H_u axis. In general, presence of more than one peak in $\rho(H_u, H_c)$ map corresponds to multiple magnetic phases. Vertical shift of the peaks characterizes the type of interaction between the phases: it is dipolar for the positive shift values while the exchange interaction appears as the negative ones.

III. EXPERIMENTAL RESULTS

We start magnetization measurements from the initially oxidized samples. Figure 1 shows magnetization loops at 100 K temperature for two CoSi crystals, 3.91 mg and 2.52 mg for (a) and (b), respectively, and the qualitative behavior is very similar. There is a weak hysteresis within ± 0.75 kOe interval of magnetic field. The main $M(H)$ dependence corresponds to the paramagnetic response, which is the known contribution of the surface Co oxides [52,53]. The sample magnetization $M(H)$ does not demonstrate any specific orientation dependence, as it is shown in the insets to Fig. 1. The shallow
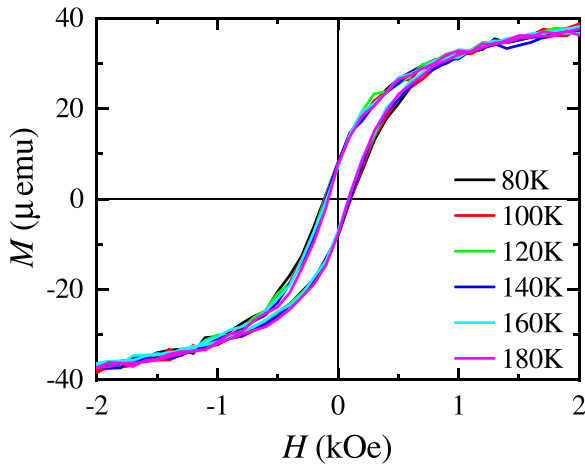
FIG. 3. The hysteresis loops for the cleaved CoSi sample from Fig. 2(a), obtained at 80 K, 100 K, 120 K, 140 K, 150 K, and 180 K temperatures. The curves are practically insensitive to temperature much below the known Curie point $T_c = 328$ K for surface ferromagnetism in CoSi [16]. This temperature dependence confirms the standard ferromagnetic behavior of the fresh CoSi surface.
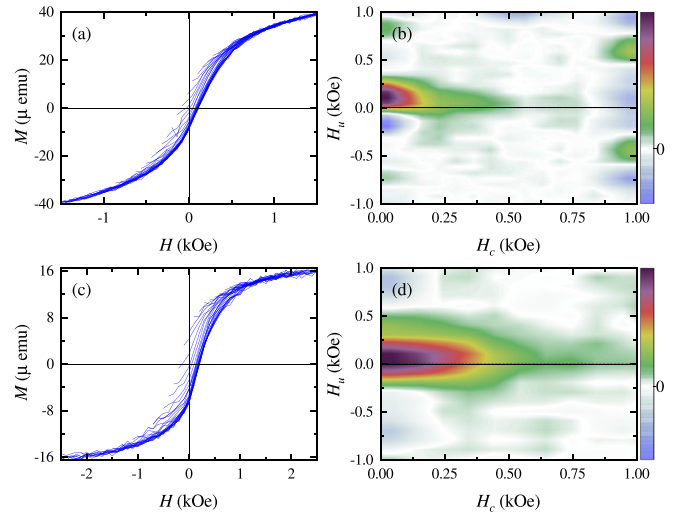

FIG. 4. (a),(c) The raw FORCs curves for two cleaved samples from Figs. 2(a) and (b), respectively, at 100 K. (b),(d) FORC density diagrams $\rho(H_u, H_c)$ for these samples. Single peak in $\rho(H_u, H_c)$ confirms a single magnetic phase in the sample, while open contours at the H_u axis indicate the multidomain regime [50,51]. Thus, a fresh CoSi surface demonstrates strong ferromagnetic multidomain behavior.

(below 5%) modulation of unstable shape is connected with the crystal facets, which can be seen in the original sample image. The signal amplitude at fixed magnetic field does not scale with the sample mass, which also correlates with the surface oxide response. Thus, the qualitative $M(H)$ behavior well-corresponds to the known one for CoSi semimetal [16,35–37].

As a second step, we repeat the magnetization measurements after cleaving the initial samples from Fig. 1 on the smaller fragments with fresh, oxide-free CoSi surface.

To our surprise, both samples demonstrate one order of magnitude increase in M value, while the sample dimensions are diminished to 1.86 mg and 0.48 mg in Figs. 2(a) and 2(b), respectively. Sample cleaving also has a dramatic effect on the qualitative $M(H)$ behavior: there is now prominent hysteresis within ± 2 kOe field range, which is accompanied by well-defined $M(H)$ saturation in higher fields. Thus, the cleaved samples demonstrate standard ferromagnetic response.

Ferromagnetic response from the fresh CoSi surface is also supported by the angle dependence of magnetization in the inset to Fig. 2(a). We observe strong modulation of the $M(\alpha)$ with 180° periodicity, as it can be expected for easy and hard axes in a ferromagnet. For the second sample in Fig. 2(b), the angle dependence is shown as two hysteresis loops for two (easy and hard) field orientations. As usual, the coercivity field is not sensitive to the field direction, while the saturation level varies within 30% of magnitude, similar to the angle dependence in the inset to Fig. 2(a).

The Curie point is above room temperature ($T_c = 328$ K) for surface ferromagnetism in CoSi [16], so the ferromagnetic response is expected to be practically insensitive to the temperature much below the Curie point, as we confirm in Fig. 3. The hysteresis loops well-coincide from 80 K to 180 K, both the loop width and the saturation level are temperature independent within this interval.

Additional information on the ferromagnetic state can be obtained from FORC data in Fig. 4. The raw FORC curves and the calculated FORC density diagram $\rho(H_u, H_c)$ are shown in Figs. 4(a), 4(c) and 4(b), 4(d), respectively, at 100 K temperature for two cleaved samples from Fig. 2. Every sample shows a single peak in $\rho(H_u, H_c)$, which is centered at low H_c values with so-called open contours at the H_u axis. This behavior is usually regarded as a fingerprint of the multidomain regime for a ferromagnet [50,51]. The peak center is slightly shifted to the positive values of the interaction field H_u, which corresponds to the dipolar interaction between domains [50,51].

IV. DISCUSSION

As a result, while the samples with oxidized surface show mostly paramagnetic response, the cleaved samples demonstrate strong ferromagnetic multidomain behavior with definite orientations for easy and hard axes. This behavior is even more surprising, since also the absolute $M(H)$ values are strongly increased for cleaved (i.e., diminished) samples.

First of all, we wish to confirm the quality of our CoSi samples. The single-phase CoSi crystal [space group P2$_1$3 (No. 198)] is confirmed by x-ray powder diffraction pattern in Fig. 5(a).

Bulk single crystals of CoSi are known to be diamagnetic with temperature-independent susceptibility [33,34]. We confirm clear diamagnetic slope in a wide magnetic field range ± 15 kOe in Fig. 5(b) for the cleaved 0.48 mg sample from Fig. 2(b). The diamagnetic slope value gives -0.8×10^6 emu/g diamagnetic susceptibility, which is in good correspondence with the previously reported data [34].

The unusual ferromagnetism was observed in CoSi single-crystal nanowires [35,36], thin polycrystalline films [16], and
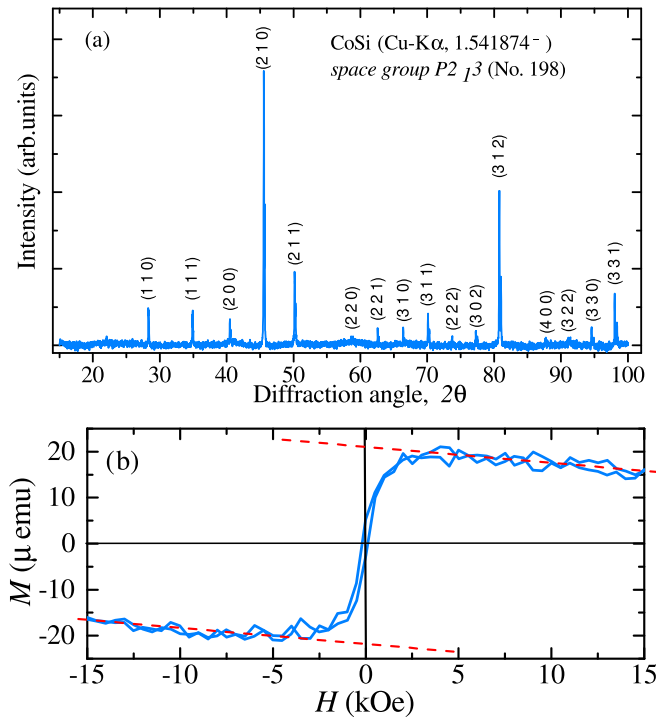
FIG. 5. Structural and magnetic characterization of our CoSi crystals. (a) The x-ray powder diffraction pattern, which is obtained for the crushed CoSi single crystal. The single-phase CoSi is confirmed with the space group P2$_1$3 (No. 198). (b) Diamagnetic (negative) slope of $M(H)$ in a wide magnetic field range ±15 kOe for the cleaved 0.48 mg sample from Fig. 2(b). The diamagnetic slope value well-corresponds to the previously reported data [34].

some bulk single crystals [37]. The origin of this ferromagnetism is still debatable.

(i) Ferromagnetic ordering can appear due to the distorted and dangling bonds near the sample surface. The transition metal (Co) d-orbital electron spin up and spin down populations become asymmetric from the exchange interactions near the CoSi surface [35,36]. In the Co (Si)-terminated (001) surface, every Co (Si) atom and the underlying Si (Co) one forms a zigzag atomic chain [14].

(ii) Another source of ferromagnetic ordering is the superlattice of defects (ordered vacancies) in CoSi single crystals [35,36]. While it is difficult to distinguish experimentally, theoretical simulations suppose that the internal ordered vacancies is the dominant contribution in CoSi single crystal nanowire ferromagnetism. [36].

(iii) Topological surface structures should also be considered for CoSi topological semimetal. The spin textures were predicted even for weakly spin-split Fermi surfaces, so the chiral cubic symmetry enforces perfectly parallel spin-momentum locking [54,55]. Skyrmion lattice has been experimentally shown for polycrystalline CoSi films [16,38,39].

Our experiment indicates that a fresh surface gives the dominant contribution to the ferromagnetism of a CoSi single crystal. Thus, the surface effects (i) and (iii) should be considered as the main reason for strong ferromagnetic behavior in Fig. 2, while we cannot exclude bulk ordered vacancies (ii) as

a source of narrow loops in Fig. 1 for the oxidized samples. To distinguish between the surface ordering mechanisms (i) and (iii), we wish to note that the structure of the distorted and dangling bonds near the sample surface can be seriously corrupted by the surface oxidation, while the topological effects (iii) are usually considered to have protection from disorder. Thus, the mechanism (i) well-corresponds to our experiment. On the other hand, one cannot expect a strong ferromagnetic response from the distorted bonds near the sample surface [35,36].

This apparent inconsistence indicates to a joint effect of the surface-induced ordering mechanisms (i) and (iii). Naturally, the RKKY interaction is expected to be available for the surface band of Weyl semimetals and, therefore, also for chiral ones [42–44]. In particular, two distorted bonds can be regarded as magnetic impurities, which are placed on the surface of the semimetal. Considering the spin-exchange interaction (s-d model) between impurities and host electrons, the system Hamiltonian can be written [42–44] as

$$H = H_{WSM} - J_0 \sum_{i=1,2} \mathbf{S}_i \mathbf{s}_i,$$

where H_{WSM} is the low-energy Hamiltonian of Weyl semimetal, J_0 is the strength of the exchange interaction, S_i is the spin of impurity at site i, and s_i refers to the spin of host electrons [44]. Mediated by the itinerant host electrons, an indirect exchange interaction (i.e., RKKY interaction) between two impurities is generated, which can be rewritten in the form of

$$H_{RKKY} = J\mathbf{S}_1\mathbf{S}_2.$$

RKKY interaction mediated by surface states in Weyl semimetals can be induced by different mechanisms [42–44]. For impurities deposited in the direction perpendicular to the Weyl points splitting, the surface contributions decay much more slowly with impurity distance than that of bulk contribution [44].

Since the topological surface states are confirmed for CoSi [5,17–19,21], the surface states-induced RKKY interaction can be responsible for the enhancement of the initially weak ferromagnetism of the distorted bonds. The latter is sensitive to the surface oxidation, while the surface states-induced RKKY interaction provides high absolute $M(H)$ values, which are strongly increased for the cleaved (i.e., significantly diminished) samples in Fig. 2.

As an additional argument, we do not observe the so-called bowtie type hysteresis loops, which are usually ascribed to skyrmions [56–59]. From the FORC data in Fig. 4, we should exclude any sizable input from the independent surface phase, since there is only a single magnetic phase for the samples with clean crystal surface. This well-correlates with the theoretical statement, that the surface states-induced RKKY interaction survives only when the surface states couple with bulk states (or other surface states of different spins) [42,43]. This does not contradict to the previous experiments, while skyrmions have been demonstrated for the polycrystalline samples only [16,38,39].

As a result, our experiment allows to distinguish between different mechanisms of the ferromagnetic ordering in CoSi single crystals, so the surface states-induced RKKY interaction between distorted and dangling bonds near the sample

surface is responsible for the strong ferromagnetic multido-main behavior with definite orientations for easy and hard axes for freshly cleaved samples.

[1] B. Bradlyn, J. Cano, Z. Wang, M. G. Vergniory, C. Felser, R. J. Cava, and B. A. Bernevig, Science **353**, aaf5037 (2016).

[2] P. Tang, Q. Zhou, and S.-C. Zhang, Phys. Rev. Lett. **119**, 206402 (2017).

[3] G. Chang, S.-Y. Xu, B. J. Wieder, D. S. Sanchez, S.-M. Huang, I. Belopolski, T.-R. Chang, S. Zhang, A. Bansil, H. Lin, and M. Z. Hasan, Phys. Rev. Lett. **119**, 206401 (2017).

[4] N. P. Armitage, E. J. Mele, and A. Vishwanath, Rev. Mod. Phys. **90**, 015001 (2018).

[5] N. B. Schröter, D. Pei, M. G. Vergniory, Y. Sun, K. Manna, F. de Juan, J. A. Krieger, V. Süss, M. Schmidt, P. Dudin, B. Bradlyn, T. K. Kim, Th. Schmitt, C. Cacho, C. Felser, V. N. Strocov, and Y. Chen, Nat. Phys. **15**, 759 (2019).

[6] D. S. Sanchez, I. Belopolski, T. A. Cochran, X. Xu, J.-X. Yin, G. Chang, W. Xie, K. Manna, V. Süss, C.-Y. Huang, N. Alidoust, D. Multer, S. S. Zhang, N. Shumiya, X. Wang, G.-Q. Wang, T.-R. Chang, C. Felser, S.-Y. Xu, S. Jia, H. Lin, and M. Zahid Hasan, Nature (London) **567**, 500 (2019).

[7] G. Chang, B. J. Wieder, F. Schindler, D. S. Sanchez, I. Belopolski, S.-M. Huang, B. Singh, D. Wu, T.-R. Chang, T. Neupert, S.-Y. Xu, H. Lin, and M. Zahid Hasan, Nat. Mater. **17**, 978 (2018).

[8] M. Zahid Hasan, G. Chang, I. Belopolski, G. Bian, S.-Y. Xu, and J.-X. Yin, Nat. Rev. Mater. **6**, 784 (2021).

[9] S. Zhong, J. E. Moore, and I. Souza, Phys. Rev. Lett. **116**, 077201 (2016).

[10] P. Rinkel, P. L. S. Lopes, and I. Garate, Phys. Rev. Lett. **119**, 107401 (2017).

[11] F. de Juan, A. G. Grushin, T. Morimoto, and J. E. Moore, Nat. Commun. **8**, 15995 (2017).

[12] S. Mühlbauer, B. Binz, F. Jonietz, C. Pfleiderer, A. Rosch, A. Neubauer, R. Georgii, and P. Bön, Science **323**, 915 (2009).

[13] A. Neubauer, C. Pfleiderer, B. Binz, A. Rosch, R. Ritz, P. G. Niklowitz, and P. Böni, Phys. Rev. Lett. **102**, 186602 (2009).

[14] Q.-Q. Yuan, L. Zhou, Z.-C. Rao, S. Tian, W.-M. Zhao, C.-L. Xue, Y. Liu, T. Zhang, C.-Y. Tang, Z.-Q. Shi, Z.-Y. Jia, H. Weng, H. Ding, Y.-J. Sun, H. Lei, S.-C. Li, Sci. Adv. **5**, eaaw9485 (2019).

[15] D. A. Pshenay-Severin and A. T. Burkov, Materials **12**, 2710 (2019).

[16] B. Balasubramanian, P. Manchanda, R. Pahari, Z. Chen, W. Zhang, S. R. Valloppilly, X. Li, A. Sarella, L. Yue, A. Ullah, P. Dev, D. A. Muller, R. Skomski, G. C. Hadjipanayis, and D. J. Sellmyer, Phys. Rev. Lett. **124**, 057201 (2020).

[17] Z. Rao, H. Li, T. Zhang, S. Tian, C. Li, B. Fu, C. Tang, L. Wang, Z. Li, W. Fan, J. Li, Y. Huang, Z. Liu, Y. Long, C. Fang, H. Weng, Y. Shi, H. Lei, Y. Sun, T. Qian et al., Nature (London) **567**, 496 (2019).

[18] D. Takane, Z. Wang, S. Souma, K. Nakayama, T. Nakamura, H. Oinuma, Y. Nakata, H. Iwasawa, C. Cacho, T. Kim, K. Horiba, H. Kumigashira, T. Takahashi, Y. Ando, and T. Sato, Phys. Rev. Lett. **122**, 076402 (2019).

[19] N. B. M. Schröter, S. Stolz, K. Manna, F. de Juan, M. G. Vergniory, J. A. Krieger, D. Pei, T. Schmitt, P. Dudin, T. K. Kim, C. Cacho, B. Bradlyn, H. Borrmann, M. Schmidt, R. Widmer, V. N. Strocov, and C. Felser, Science **369**, 179 (2020).

[20] S.-Y. Xu, I. Belopolski, D. S. Sanchez, M. Neupane, G. Chang, K. Yaji, Z. Yuan, C. Zhang, K. Kuroda, G. Bian, C. Guo, H. Lu, T.-R. Chang, N. Alidoust, H. Zheng, C.-C. Lee, S.-M. Huang, C.-H. Hsu, H.-T. Jeng, A. Bansil et al., Phys. Rev. Lett. **116**, 096801 (2016).

[21] D. A. Pshenay-Severin, Y. V. Ivanov, A. A. Burkov, and A. T. Burkov, J. Phys.: Condens. Matter **30**, 135501 (2018).

[22] S.-X. Wang, H.-R. Chang, and J. Zhou, Phys. Rev. B **96**, 115204 (2017).

[23] H.-R. Chang, J. Zhou, S.-X. Wang, W.-Y. Shan, and D. Xiao, Phys. Rev. B **92**, 241103(R) (2015).

[24] M. M. Valizadeh, Int. J. Mod. Phys. B **30**, 1650234 (2016).

[25] J.-J. Zhu, D.-X. Yao, S.-C. Zhang, and K. Chang, Phys. Rev. Lett. **106**, 097201 (2011).

[26] K. Everschor-Sitte, J. Masell, R. M. Reeve, and M. Klaui, J. Appl. Phys. **124**, 240901 (2018).

[27] Y. Y. Dai, H. Wang, P. Tao, T. Yang, W. J. Ren, and Z. D. Zhang, Phys. Rev. B **88**, 054403 (2013).

[28] C. Back et al., J. Phys. D **53**, 363001 (2020).

[29] J. Kang and J. Zang, Phys. Rev. B **91**, 134401 (2015).

[30] B. A. Bernevig, J. Orenstein, and S.-C. Zhang, Phys. Rev. Lett. **97**, 236601 (2006).

[31] J. D. Koralek et al., Nature (London) **458**, 610 (2009).

[32] Y. Fang, S. Ran, W. Xie, S. Wang, Y. S. Meng, and M. Brian Maple, Proc. Natl. Acad. Sci. USA **115**, 8558 (2018).

[33] D. Shinoda and S. Asanabe, J. Phys. Soc. Jpn. **21**, 555 (1966).

[34] S. M. Stishov, A. E. Petrova, V. A. Sidorov, and D. Menzel, Phys. Rev. B **86**, 064433 (2012).

[35] K. Seo, K. S. K. Varadwaj, P. Mohanty, S. Lee, Y. Jo, M.-H. Jung, J. Kim, and B. Kim, Nano Lett. **7**, 1240 (2007).

[36] T.-K. Liu, C.-T. Lee, S.-H. Chiou, Y.-W. Hsu, J. van Lierop, and Chuenhou (Hao) Ouyang, Nanotechnology **26**, 065707 (2015).

[37] V. N. Narozhnyi and V. N. Krasnorussky, J. Exp. Theor. Phys. **116**, 780 (2013).

[38] X. Yao, Y. Wang, and S. Dong, Int. J. Mod. Phys. B **35**, 2130004 (2021).

[39] N. Nagaosa and Y. Tokura, Nat. Nanotechnol. **8**, 899 (2013).

[40] V. D. Esin, A. V. Timonina, N. N. Kolesnikov, and E. V. Deviatov, J. Magn. Magn. Mater. **540**, 168488 (2021).

[41] D. S. Sanchez, T. A. Cochran, I. Belopolski, Z.-J. Cheng, X. P. Yang, Y. Liu, X. Xu, K. Manna, J.-X. Yin, H. Borrmann, A. Chikina, J. Denlinger, V. N. Strocov, C. Felser, S. Jia, G. Chang, and M. Zahid Hasan, arXiv:2108.13957.

[42] H.-J. Duan, S.-H. Zheng, P.-H. Fu, R.-Q. Wang, J.-F. Liu, G.-H. Wang, and M. Yang, New J. Phys. **20**, 103008 (2018).

[43] V. Kaladzhyan, A. A. Zyuzin, and P. Simon, Phys. Rev. B **99**, 165302 (2019).

[44] H.-J. Duan, Y.-J. Wu, M.-X. Deng, R. Wang, and M. Yang, arXiv:2211.12350.

[45] V. D. Esin, Yu. S. Barash, A. V. Timonina, N. N. Kolesnikov, and E. V. Deviatov, JETP Lett. **113**, 662 (2021).

[46] V. D. Esin, A. V. Timonina, N. N. Kolesnikov, and E. V. Deviatov, J. Exp. Theor. Phys. **133**, 792 (2021).

[47] B. C. Dodrill, Magnetometry Measurements and First-Order-Reversal-Curve (FORC) Analysis, Lake Shore Cryotronics, www.lakeshore.com.

[48] D. A. Gilbert, P. D. Murray, J. De Rojas, R. K. Dumas, J. E. Davies, and K. Liu, Sci. Rep. **11**, 4018 (2021).

[49] A. A. Avakyants, N. N. Orlova, A. Timonina, N. N. Kolesnikov, E. V. Deviatov, J. Magn. Magn. Mater **573**, 170668 (2023).

[50] B. C. Dodrill, H. S. Reichard, and T. Shimizu, Lake Shore Cryotronics. Technical Note. www.lakeshore.com.

[51] B. C. Dodrill, TechConnect Briefs **1**, 32 (2018).

[52] N. Kernavanois, E. Ressouche, P. J. Brown, J. Y. Henry, and E. Lelièvre-Berna, Phys. B: Condens. Matter **350**, E265 (2004).

[53] Y. Koseoglu, F. Kurtulus, H. Kockar, H. Guler, O. Karaagac, S. Kazan, and B. Aktas, J. Supercond. Nov. Magn. **25**, 2783 (2012).

[54] C. Mera Acosta, L. Yuan, G. M. Dalpian, and A. Zunger, Phys. Rev. B **104**, 104408 (2021).

[55] W. Tan, X. Jiang, Y. Li, X. Wu, J. Wang, and B. Huang, Adv. Funct. Mater. **32**, 2208023 (2022).

[56] S. Zhang, J. Zhang, Y. Wen, E. M. Chudnovsky, and X. Zhang, Commun. Phys. **1**, 36 (2018).

[57] Y. Ba, S. Zhuang, Y. Zhang, Y. Wang, Y. Gao, H. Zhou, M. Chen, W. Sun, Q. Liu, G. Chai, J. Ma, Y. Zhang, H. Tian, H. Du, W. Jiang, C. Nan, J.-M. Hu, and Y. Zhao, Nat. Commun. **12**, 322 (2021).

[58] R. Streubel, L. Han, M.-Y. Im, F. Kronast, U. K. Röler, F. Radu, R. Abrudan, G. Lin, O. G. Schmidt, P. Fischer, and D. Makarov, Sci. Rep. **5**, 8787 (2015).

[59] A. Soumyanarayanan, M. Raju, A. L. Gonzalez Oyarce, A. K. C. Tan, M.-Y. Im, A. P. Petrović, P. Ho, K. H. Khoo, M. Tran, C. K. Gan, F. Ernult, and C. Panagopoulos, Nat. Mater. **16**, 898 (2017).